Journal of Physics: Conference Series **1468** (2020) 012235 doi:10.1088/1742-6596/1468/1/012235

A measurement of the scintillation decay time constant in liquid xenon with the XMASS-I detector

K. Ichimura for the XMASS Collaboration

Kamioka Observatory, Institute for Cosmic Ray Research, the University of Tokyo, Higashi-Mozumi, Kamioka, Hida, Gifu, 506-1205, Japan
Kavli Institute for the Physics and Mathematics of the Universe (WPI), the University of Tokyo, Kashiwa, Chiba, 277-8582, Japan

E-mail: ichimura@km.icrr.u-tokyo.ac.jp

Abstract. The scintillation decay time constant in liquid xenon was measured using the XMASS-I detector and its calibration setup. The scintillation decay time constants of both electron recoil and nuclear recoil were evaluated by comparing the observed photon detection times with Monte Carlo simulations. Two exponential components, corresponding to the singlet and triplet state of the xenon excited dimer, are needed to reproduce the observed photon detection times. In this paper, we report the measurement of the electron recoil and the nuclear recoil scintillation decay time constants with the XMASS-I detector.

1. Introduction

Liquid xenon (LXe) has been used in many modern experiments for rare event searches - such as dark matter [1] - thanks to its high ionization and scintillation yield as well as high atomic number and density that enable us to reduce external background. Scintillation photons from LXe are produced via two mechanisms. One is the direct excitation of Xe atoms and the other is the recombination process between electrons and Xe ions. Both processes eventually form an excited dimer Xe_2^* that has both a singlet and a triplet state. The decay time constant of the singlet and triplet states were reported to be a few ns and about 20 ns, respectively [2, 3, 4, 5]. The recombination process has a longer additional decay time constant of more than 30 ns, measured with 1 MeV electrons from a ^{207}Bi source [2, 6]. The singlet state to triplet state Xe_2^* dimer ratio as well as the recombination time depends on the deposited energy density [7]. Therefore, time profiles constructed from the observed scintillation photons for each event may be useful in discriminating between nuclear recoil (NR) events and electron recoil (ER) events. In XMASS-I, we measured a distinct scintillation decay time constant for ER and for NR in LXe using calibration sources. In the following sections, we report the detector, calibration setup, analysis method and result of the measurement of these scintillation decay time constants.

2. XMASS-I detector and the calibration setup

2.1. XMASS-I detector

The XMASS detector is located in the Kamioka mine in Japan. The inner detector (ID) contains about 832 kg of LXe inside an oxygen free high conductivity copper pentakis-dodecahedron structure with a diameter of roughly 80 cm. Scintillation light from LXe is detected by 630

hexagonal 2-inch Hamamatsu R10789 photomultiplier tubes (PMTs) and 12 cylindrical 2-inch R10789mod PMTs. The ID is placed at the center of an outer detector (OD) 10 m in diameter and 10.5 m height filled with pure water to reduce the external background. 72 Hamamatsu 20-inch R3600 PMTs are mounted on the inner surface of the water tank to provide an active muon veto. Signals from the 642 ID PMTs are recorded by CAEN V1751 waveform digitizers with a 1 GHz sampling rate and 10-bit resolution. More details of the XMASS-I detector can be found in Ref. [1].

2.2. The calibration setup

For the measurement of the ER scintillation decay time constant, radioactive sources of ^{55}Fe, ^{241}Am and ^{57}Co were used. The detail of the calibration source is in Ref. [8]. These radioactive sources were inserted into the detector along its vertical axis. As for NR, a ^{252}Cf source was deployed through the stainless steel pipe. Figure 1 shows the schematic view of the XMASS detector and the ^{252}Cf calibration setup. ^{252}Cf undergoes spontaneous fission and emits about 3.7 neutrons and 8 gammas per fission. To detect the gamma-rays, the plastic scintillator BC400 was used. Timing coincidence between plastic scintillator and XMASS ID allows us to collect NR events effectively.

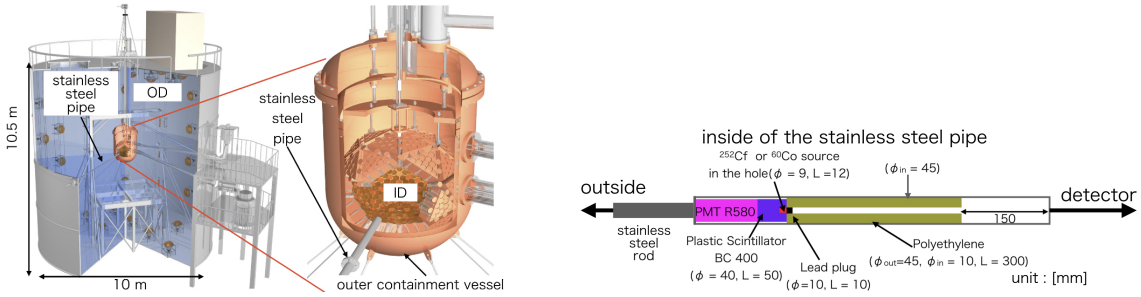

Figure 1. Schematic view of the XMASS detector (left) and the calibration setup (right). This figure is taken from Ref. [9].

3. Analysis method

The scintillation time profile for both ER and NR is evaluated by comparing the reconstructed pulse timing distribution over all PMTs of data and Monte Carlo (MC) simulation with various timing parameters. The MC simulation is developed by us and based on Geant4 [10]. It contains a detailed detector geometry, particle tracking, LXe scintillation process, photon tracking, PMT response and the electronics response. The i^{th} scintillation photon time of observation T^i in the MC simulation is defined as

$$T^i = t_{\text{Edep}} + t^i_{\text{scinti}} + t^i_{\text{TOF}} + t^i_{\text{TT}} + t^i_{\text{jitter}}. \tag{1}$$

Here t_{Edep} is the time when the incident particle deposits its energy in the LXe. t^i_{TOF} is the time of flight of the scintillation photon. t^i_{TT} is the transit time within the PMT, which we assume to be the same for all PMTs. The transit time spread t^i_{TT} of $\sigma = 2.4$ ns [11] is included in the timing calculation. t^i_{jitter} is a smearing parameter accounting for the timing jitter in the electronic channel of PMT and extracted from the ^{57}Co calibration data. It follows a Gaussian distribution with a standard deviation of 0.93 ns [12]. We found that the LXe scintillation photon emission time t^i_{scinti} follows the double exponential scintillation decay time profile:

$$f(t) = \frac{F_S}{\tau_S} \cdot \exp\left(-\frac{t}{\tau_S}\right) + \frac{1 - F_S}{\tau_T} \cdot \exp\left(-\frac{t}{\tau_T}\right). \tag{2}$$

τ_S and τ_T correspond to the decay constants of the singlet and the triplet states with the effect of the recombination process, respectively. F_S corresponds to the fraction of photons generated from decays of singlet dimers. After calculating T^i for all photons, a waveform for each PMT was simulated using the one PE pulse shape extracted from LED calibration data. To analyse each PMT's waveform, a peak finding algorithm based on a Savitzky-Golay filter [13] was developed to obtain individual photon arrival times. For each event, the photon arrival times of all peaks within all PMTs are extracted and time ordered. Next, the timing of the fourth earliest peak is set to T = 0 ns with all other peak times within the event shifted relative to this time, reflecting the trigger implementation in the data acquisition. This allows for all recorded peak times within multiple events to be superposed and is applied to both data and MC simulation. The scintillation decay time constant is obtained by performing the following χ^2 fit:

$$\chi^2 = \sum_i \frac{(N_i^{\rm data} - N_i^{\rm MC} \times S)^2}{N_i^{\rm data} + N_i^{\rm MC} \times S^2} \tag{3}$$

Here $N_i^{\rm data}$ and $N_i^{\rm MC}$ are the number of pulses in the i-th time bin for data and MC simulation, respectively. Each time bin is 1 ns wide and the χ^2 is calculated using the 3 ns $\leq T \leq$ 120 ns time bins. F_S and τ_T are scanned while fixing the τ_S = 2.2 $\pm$ 0.3 ns[14] for ER and τ_S = 4.3 $\pm$ 0.6 ns for NR [2]. Figure 2 shows the pulse timing distribution of data and the best fit MC simulation for ^{241}Am calibration and ^{252}Cf calibration. The MC simulation cannot reproduce the timing distribution of the data without the contribution of a fast decay component. We obtained the decay time constant of (τ_T, F_S) = ($31.9^{+1.2}_{-1.5}$ ns, $0.048^{+0.017}_{-0.019}$) for ^{241}Am 59.5 keV gamma-ray events and ($26.9^{+0.7}_{-1.1}$ ns, $0.252^{+0.027}_{-0.019}$), for NR events in the energy range from 1.5 keV$_{\rm ee}$ to 8.3 keV$_{\rm ee}$, respectively. Figure 3 shows τ_T and F_S for various NR and ER measurements. This measurement has the lowest energy threshold of all the experiments conducted without an external electric field.

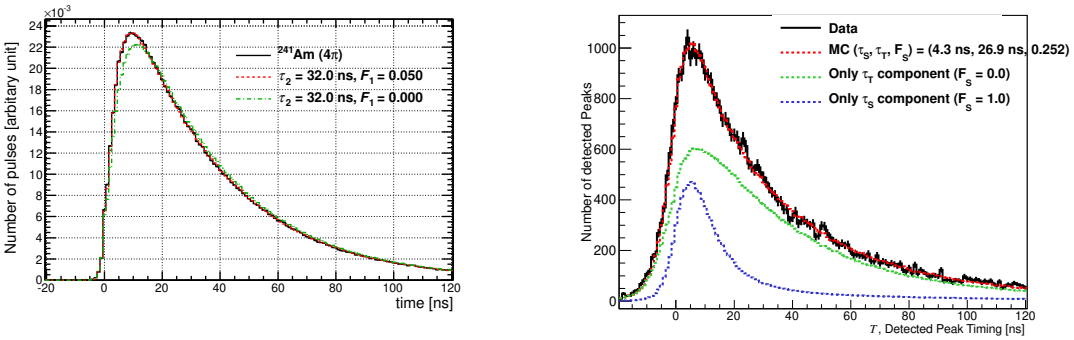

Figure 2. The pulse timing distribution of the observed data (black) overlaid with those of the best fit simulated samples (red) for ^{241}Am 59.5 keV gamma-rays (left) and ^{252}Cf NR events (right). The fit region is 3 ns $\leq T \leq$ 120 ns. These figures are taken from Ref. [9, 12].

4. Summary

We have measured the scintillation decay time constant of both ER and NR with the XMASS-I detector. Two decay components are needed to reproduce the pulse timing distribution of both the ER and NR data. The detailed analysis of the decay time constant of ER is published in [12], and that of NR and the prospects for pulse shape discrimination are published in [9].

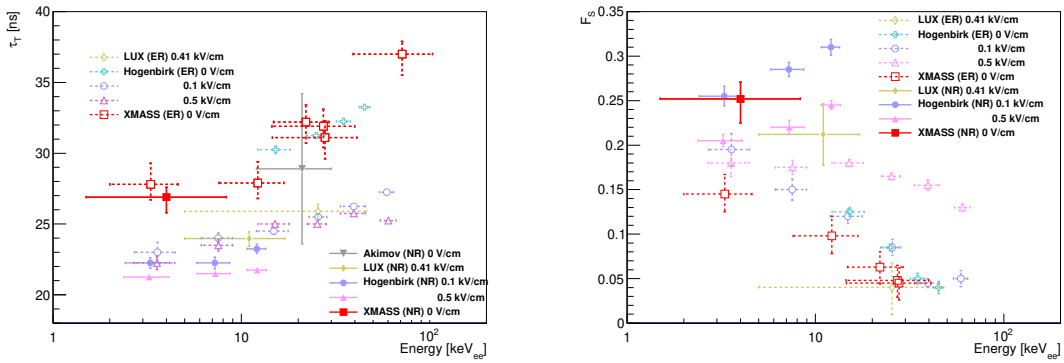

Figure 3. The best-fit parameters τ_T and F_S for various measurements. Filled markers and solid lines correspond to NR measurements. Open markers and dotted lines correspond to ER measurements. Results from Akimov et al. [5], the LUX experiment [3], Hogenbirk et al. (0 V/cm, 0.1 kV/cm and 0.5 kV/cm) [4], and XMASS measurements ([9] and [12]) are indicated by a gray triangle, cyan crosses, yellow diamonds, green crosses, blue circles, magenta triangles, and red squares, respectively. These figures are taken from Ref. [9].

5. Acknowledgments

We gratefully acknowledge the cooperation of the Kamioka Mining and Smelting Company. This work was supported by the Japanese Ministry of Education, Culture, Sports, Science and Technology, Grant-in-Aid for Scientific Research, JSPS KAKENHI Grant No. 19GS0204, 26104004, and 19H05805, the joint research program of the Institute for Cosmic Ray Research (ICRR), the University of Tokyo, and partially by the National Research Foundation of Korea Grant funded by the Korean Government (NRF-2011-220-C00006), and Institute for Basic Science (IBS-R017-G1-2018-a00).

6. References

[1] K. Abe *et al.*, Nucl. Instrum. Meth. A716 (2013) 78–85.
[2] A. Hitachi *et al.*, Phys. Rev. B27 (1983) 5279–5285.
[3] D. S. Akerib *et al.* (LUX), Phys. Rev. D97 (11) (2018) 112002.
[4] E. Hogenbirk *et al.*, JINST 13 (05) (2018) P05016.
[5] D. Akimov *et al.*, Phys. Lett. B524 (2002) 245–251.
[6] S. Kubota *et al.*, Phys. Rev. B20 (8) (1979) 3486.
[7] E. Aprile, T. Doke, Rev. Mod. Phys. 82 (2010) 2053–2097.
[8] N. Y. Kim *et al.*, Nucl. Instrum. Meth. A784 (2015) 499–503.
[9] K. Abe *et al.* (XMASS), JINST 13 (12) (2018) P12032.
[10] S. Agostinelli *et al.* (GEANT4), Nucl. Instrum. Meth. A506 (2003) 250–303.
[11] H. Uchida *et al.* (XMASS-I), PTEP 2014 (6) (2014) 063C01.
[12] H. Takiya *et al.* (XMASS), Nucl. Instrum. Meth. A834 (2016) 192–196.
[13] A. Savitzky, M. J. E. Golay, NAnal. Chem. 36 (1964) 1627–1639.
[14] S. Kubota, M. Hishida, J. Raun, Journal of Physics C: Solid State Physics 11 (12) (1978) 2645–2651.